Acta Acustica united with Acustica
Vol. 104 (2018) 235 – 242

DOI 10.3813/AAA.919165

Second-Harmonic Generation in Acoustic Waveguides Loaded with an Array of Side Holes

Jiangyi Zhang[1)], Vicente Romero-García[1)], Georgios Theocharis[1)], Olivier Richoux[1)], Vassos Achilleos[1)], Dimitrios J. Frantzeskakis[2)]

[1)] Laboratoire d'Acoustique de l'Université du Maine – CNRS UMR 6613, Le Mans, France. Jiangyi.Zhang.Etu@univ-lemans.fr

[2)] Department of Physics, National and Kapodistrian University of Athens, Panepistimiopolis, Zografos, Athens 15784, Greece

Summary

We study analytically and numerically second-harmonic generation in a one-dimensional weakly lossy nonlinear acoustic metamaterial composed of an air-filled waveguide periodically loaded by side holes. Based on the transmission line approach, we derive a lossy nonlinear dispersive lattice model which, in the continuum limit, leads to a nonlinear, dispersive and dissipative wave equation. The latter is studied by means of a perturbation method, which leads to analytical expressions for the first and second harmonics, in very good agreement with numerical results.

PACS no. 43.25.-x, 43.25.Jh

1. Introduction

The study of metamaterials in different fields of wave physics has seen an explosion of interest during the last years, leading to significant developments both from basic research and applications point of view. Metamaterials are artificially engineered structures, exhibiting physical properties not found in nature [1, 2, 3]. In the case of acoustics, Liu *et al.* [4] proposed the first acoustic metamaterial, originally called locally resonant sonic material, based on an array of coated spheres presenting negative mass density. Later, Fang *et al.* [5] investigated an acoustic metamaterial composed by an array of Helmholtz resonators embedded in a waveguide, presenting negative bulk modulus. Although such systems have been previously analyzed in the context of acoustics by Sugimoto [6] and Bradley [7], the novelty in this case is to characterize the system by using the effective properties. The linear properties of such acoustic metamaterials including the effect of viscothermal losses [8] have been exploited over the last decade, showing several possibilities to control wave propagation in acoustics [9, 10, 11, 12, 13, 14, 15, 16].

In addition to the more standard case of linear metamaterials, the study of nonlinear ones has been receiving increased attention during the last years [17, 18, 19, 20]. However, in the case of acoustic metamaterials, the presence of nonlinearity is less studied, and only a few works have exploited the combined role nonlinear effects and other fundamental features of the system, such as dispersion or losses. The combination of nonlinearity and dispersion has revealed different effects, such as the formation of solitons [21, 22, 23], the self-demodulation effect [24, 25] and the generation of higher harmonics [26, 27, 28]. More recently, in a similar setup with negative mass density, the formation of envelope (bright and gap) solitons has been analytically and numerically studied in the presence of viscothermal losses [29].

In this work, we analytically and numerically study the second-harmonic generation in an one-dimensional (1D) weakly lossy nonlinear acoustic metamaterial with negative bulk modulus composed by an air-filled waveguide periodically loaded by side holes. The main motivation is to study the combined effects of dispersion, nonlinearity and dissipation in an acoustic metamaterial with negative bulk modulus (our setup). The model used in this work could pave the way to study the linear and nonlinear propagation in double negative metamaterials considering the different physical effects playing role as dispersion, nonlinearity and dissipation. The nonlinearity is activated here by using high-amplitude incident waves. Based on the electro-acoustic analogy and the transmission line approach, we derive a weakly lossy lattice model describing the system, which, in the continuum limit, leads to a nonlinear, dispersive and dissipative wave equation. By using a perturbative scheme we derive analytical expressions for the first and second harmonics, in the presence of losses. The analytical results are found to be in very good agreement with direct numerical simulations in the framework of the lattice model.

Received 25 August 2017,
accepted 27 November 2017.

The article is structured as follows. In Section 2 we introduce the electro-acoustic analogue modeling based on the transmission line (TL) approach, which has been shown to be a powerful tool for studying electromagnetic and acoustic metamaterials [29, 30, 31, 32, 33, 34]. In Section 2.1, we describe the setup and introduce the 1D nonlinear dissipative lattice model. Then, in Section 2.2, we obtain a nonlinear dispersive and dissipative wave equation, stemming from the continuum limit of the lattice model. Section 2.3 describes the linear properties of the proposed metamaterial. In Section 3, we present the analytical and numerical results regarding the second harmonic generation. Finally, in Section 4, we summarize and present our conclusions.

2. Electro-Acoustic Analogue Modeling

2.1. Setup and model

We consider low-frequency nonlinear wave propagation in the acoustic metamaterial shown in Figure 1a. The structure is composed by a waveguide of radius r periodically loaded with an array of side holes of radius r_H and length l_H. The distance between two consecutive side holes is d. The frequency range considered is well below the first cut-off frequency, therefore the problem is considered as one-dimensional.

We adopt the electro-acoustic analogy, where the voltage corresponds to the acoustic pressure and the current to the volume velocity flowing through the waveguide's cross-sectional area [35, 36]. Our aim is to derive a nonlinear discrete wave equation, describing wave propagation in an equivalent electrical transmission line (TL). To do this, we consider the unit-cell circuit of the equivalent TL model of our setting, shown in Figure 1b.

The unit-cell circuit is composed by two parts. The first one, corresponding to the waveguide, is modeled by the acoustic masses M_ω, the resistance R_ω and shunt acoustic compliances C_ω. In the linear regime, the acoustic masses and acoustic compliances are given by $M_{\omega 0} = \rho_0 d/S$ and $C_{\omega 0} = Sd/(\rho_0 c_0^2)$, where ρ_0, c_0 and S are respectively the density, the speed of sound and the cross-section area of the waveguide. The resistance $R_\omega = \mathrm{Im}(kZ_c)d$ describes the viscothermal losses, where the wavenumber and acoustic characteristic impedance of the waveguide are given by [8]:

$$k = \frac{\omega}{c_0}\left(1 + \frac{1-j}{s}(1 + (\gamma - 1)/\sqrt{Pr})\right), \qquad (1)$$

$$Z_c = \frac{\rho_0 c_0}{S}\left(1 + \frac{1-j}{s}(1 - (\gamma - 1)/\sqrt{Pr})\right). \qquad (2)$$

Here, γ is the specific heat ratio, Pr is the Prandtl number, and $s = \sqrt{\omega\rho_0 r^2/\eta}$, with η being the shear viscosity.

The second part of the unit-cell circuit, corresponding to the side hole, is modeled by a shunt RM circuit composed by the series combination of an acoustic masses M_H and a resistance R_H. In the regime where the geometric characteristics of the side holes are much smaller than the wavelength λ of the sound wave, i.e., for $kr_H \ll 1$, the corresponding acoustic masses and resistance are given by $M_H = \rho_0 l_H/S_H$ and $R_H = \rho_0\omega^2/(2\pi c_0)$, where S_H is the area of the side holes [37]. Here we should mention that we approximate the frequency-dependent viscothermal and radiation losses by a resistance with a constant value at the frequency of the wave excitation (cf. see last two paragraphs in Section 2.3 for more details).

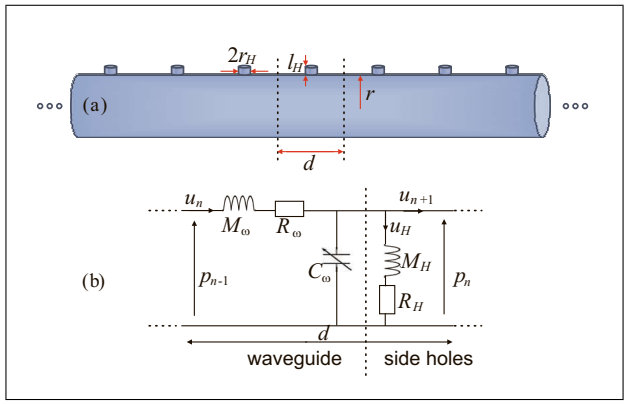

Figure 1. (Colour online) (a) Acoustic metamaterials composed by a waveguide loaded with an array of side holes. (b) Corresponding unit-cell circuit.

Here, we should mention that we consider the response of side holes to be linear while the propagation in the waveguide weakly nonlinear. At high acoustic level, generally the response of the side holes is nonlinear due to nonlinear losses as a consequence of a jet formation at the locations of the side holes and the formation of annular vortices dissipating part of the acoustic energy. However, these effects can be minimized considering holes with smoothed walls [38, 39]. Therefore the assumption of the linear behavior of the holes is a good approximation as far as the boundaries of the holes are smoothed, an aspect that has to be taken into account in the design of the experimental setup. On the other hand, it is well known that, due to the compressibility of air, the wave celerity c_{NL} is considered amplitude dependent and thus the propagation in the waveguide weakly nonlinear.

Therefore, we assume the acoustic compliances C_a to be nonlinear, depending on the pressure p [23], while the acoustic masses M_a linear. Approximating the celerity as $c_{NL} \approx c_0\left(1 + \beta_0 p/\rho_0 c_0^2\right)$, where β_0 is the nonlinear parameter for the case of air, the pressure-dependent acoustic compliances C_ω can be expressed as $C_\omega = C_{\omega 0} - C_\omega^{'} p_n$, where

$$C_\omega^{'} = \frac{2\beta_0}{\rho_0 c_0^2} C_{\omega 0}. \qquad (3)$$

Next, we use Kirchhoff's voltage and current laws to derive an evolution equation for the pressure p_n in the n-th cell of the lattice. In particular, Kirchhoff's voltage law for two successive cells yields

$$p_{n-1} - p_n = M_\omega \frac{\mathrm{d}}{\mathrm{d}t} u_n + R_\omega u_n, \qquad (4)$$

$$p_n - p_{n+1} = M_\omega \frac{\mathrm{d}}{\mathrm{d}t} u_{n+1} + R_\omega u_{n+1}. \tag{5}$$

Subtracting the two equations above, we obtain the differential-difference equation (DDE),

$$\hat{\delta}^2 p_n = \left(M_\omega \frac{\mathrm{d}}{\mathrm{d}t} + R_\omega \right) (u_n - u_{n+1}), \tag{6}$$

where $\hat{\delta}^2 p_n \equiv p_{n+1} - 2p_n + p_{n-1}$. Then, Kirchhoff's current law yields

$$u_n - u_{n+1} = C_\omega \frac{\mathrm{d}}{\mathrm{d}t} p_n + u_H, \tag{7}$$

where u_H is the current through $M_H R_H$ branch. The auxiliary Kirchoff's voltage law in the output loop of the unit-cell circuit reads

$$u_H = \hat{Q}^{-1} p_n, \quad \hat{Q} = M_H \frac{\mathrm{d}}{\mathrm{d}t} + R_H. \tag{8}$$

Then, substituting Equation (7) and Equation (8) into Equation (6), and recalling that the acoustic compliances C_ω depends on the pressure, we obtain the following evolution equation for the pressure,

$$\begin{aligned} &\left(M_H \frac{\mathrm{d}}{\mathrm{d}t} + R_H \right) \\ &\left(\hat{\delta}^2 p_n - M_\omega C_{\omega 0} \frac{\mathrm{d}^2 p_n}{\mathrm{d}t^2} - R_\omega C_{\omega 0} \frac{\mathrm{d}p_n}{\mathrm{d}t} \right. \\ &\quad \left. + \frac{1}{2} M_\omega C_\omega' \frac{\mathrm{d}^2 p_n^2}{\mathrm{d}t^2} + \frac{1}{2} R_\omega C_\omega' \frac{\mathrm{d}p_n^2}{\mathrm{d}t} \right) \\ &\qquad - \left(M_\omega \frac{\mathrm{d}}{\mathrm{d}t} + R_\omega \right) p_n = 0. \end{aligned} \tag{9}$$

Our results are obtained for a temperature of 18° C and an air-filled waveguide. We use the following parameter values: $d = 0.05$ m, $r = 0.025$ m, $r_H = 0.0025$ m and $l_H = 0.005$ m, $\beta_0 = 1.2$, $c_0 = 343.26$ m/s, $\rho_0 = 1.29$ kg/m^3, $\gamma = 1.4$, $Pr = 0.71$, $\eta = 1.84\ 10^{-5}$ kg/m/s.

2.2. Continuum limit

For our analytical considerations, we focus on the continuum limit of Equation (9), corresponding to $n \to \infty$ and $d \to 0$ (but with nd being finite); in such a case, the pressure becomes $p_n(t) \to p(x,t)$, where $x = nd$ is a continuous variable, and

$$\begin{aligned} p_{n\pm1} = p &\pm d \frac{\partial p}{\partial x} + \frac{d^2}{2} \frac{\partial^2 p}{\partial x^2} \\ &\pm \frac{d^3}{3!} \frac{\partial^3 p}{\partial x^3} + \frac{d^4}{4!} \frac{\partial^4 p}{\partial x^4} + O(d^5). \end{aligned} \tag{10}$$

Thus, the difference operator $\hat{\delta}^2$ is approximated by $\hat{\delta}^2 p_n \approx d^2 p_{xx} + d^4 p_{xxxx}/12$, where subscripts denote partial derivatives, and terms of the order $O(d^5)$ and higher are neglected. This way, Equation (9) turns to the following partial differential equation (PDE),

$$\begin{aligned} &\left(M_H \frac{\partial}{\partial t} + R_H \right) \left(d^2 \frac{\partial^2 p}{\partial x^2} + \frac{d^4}{12} \frac{\partial^4 p}{\partial x^4} - M_\omega C_{\omega 0} \frac{\partial^2 p}{\partial t^2} \right. \\ &\quad \left. - R_\omega C_{\omega 0} \frac{\partial p}{\partial t} + \frac{1}{2} M_\omega C_\omega' \frac{\partial^2 p^2}{\partial t^2} + \frac{1}{2} R_\omega C_\omega' \frac{\partial p^2}{\partial t} \right) \\ &\qquad - \left(M_\omega \frac{\partial}{\partial t} + R_\omega \right) p = 0. \end{aligned} \tag{11}$$

It is convenient to express our model in a dimensionless form using the normalized variables τ, χ, and p, which are defined as follows: τ is time in units of ω_B^{-1}, where $\omega_B = \pi c_0/d$ is the Bragg frequency; χ is space in units of c_0/ω_B and $p/P_0 = \epsilon P$, where $P_0 = \rho_0 c_0^2$ and $0 < \epsilon \ll 1$ is a formal small parameter. Then, Equation (11) is expressed in the following dimensionless form,

$$\begin{aligned} &(\partial_\tau + \gamma_H) \left[P_{\tau\tau} - P_{\chi\chi} - \zeta P_{\chi\chi\chi\chi} + \gamma_\omega P_\tau \right. \\ &\left. \quad - \epsilon\beta_0 (P^2)_{\tau\tau} - \epsilon\beta_0\gamma_\omega (P^2)_\tau \right] + m^2 P_\tau + m^2 \gamma_\omega P = 0, \end{aligned} \tag{12}$$

where

$$\begin{aligned} m^2 &= \frac{S_H d}{\pi^2 l_H S}, \qquad \zeta = \frac{\pi^2}{12}, \\ \gamma_H &= \frac{R_H}{\omega_B M_H}, \quad \gamma_\omega = \frac{R_\omega S}{\pi \rho_0 c_0}. \end{aligned} \tag{13}$$

It is interesting to identify various limiting cases of Equation (12). First, in the linear limit ($\beta_0 = 0$, or $p^2 \ll 1$), in the absence of side holes ($m^2 \to 0$, $\gamma_H \to 0$), without considering viscothermal losses ($\gamma_\omega \to 0$) and higher order spatial derivatives, Equation (12) is reduced to the linear wave equation, $P_{\tau\tau} - P_{\chi\chi} = 0$. In the linear limit, but in the presence of side holes, in the long wavelength approximation and without considering viscothermal losses ($\gamma_\omega \to 0$), radiation losses ($\gamma_H \to 0$), and higher order spatial derivatives ($\zeta \to 0$), Equation (12) takes the form of the linear Klein-Gordon equation [40, 41], $P_{\tau\tau} - P_{\chi\chi} + m^2 P = 0$. Finally, including only the nonlinearity and discarding losses, the side holes, and higher order spatial derivatives, Equation (12) is reduced to the well-known Westervelt equation, $P_{\tau\tau} - P_{\chi\chi} - \epsilon\beta_0 \left(P^2\right)_{\tau\tau} = 0$, which is a common nonlinear model describing 1D acoustic wave propagation [42].

2.3. Linear limit

We first study the linear limit of Equation (12) and the respective dispersion relation. Assuming the propagation of plane waves, of the form $p \propto \exp[i(k\chi - \omega\tau)]$, we obtain the following dispersion relation connecting the wavenumber k and frequency ω,

$$\begin{aligned} D(\omega, k) = &-\mathrm{i}\omega(-\omega^2 + k^2 - \zeta k^4 + m^2) \\ &- \mathrm{i}\omega\gamma_H\gamma_\omega + \gamma_H(-\omega^2 + k^2 \\ &- \zeta k^4) + \gamma_\omega(-\omega^2 + m^2) = 0, \end{aligned} \tag{14}$$

where the terms including γ_H and γ_ω accounts for the radiation and viscothermal losses. The term ζk^4 accounts for

the influence of the periodicity of the lattice (originating from the term $\hat{\delta}^2 p_n$) to the dispersion relation. Although this term appears to lead to instabilities for large values of k, both Equation (12) and Equation (14) are used in our analysis only in the long-wavelength limit, where k is sufficiently small. Without considering the losses and higher-order spatial derivatives, Equation (14) is reduced to $-\omega^2 + k^2 + m^2 = 0$, the familiar dispersion relation of the linear Klein-Gordon model [40, 41]. For low frequencies, i.e., for $0 \leq \omega < m$, there is a band gap, and for $m < \omega < \omega_B$, there is a pass band, with the dispersion curve $\omega(k)$ having the form of hyperbola.

Since all quantities in the above dispersion relation are dimensionless, it is also relevant to express them in physical units. In particular, taking into regard that the frequency ω_{ph} and wavenumber k_{ph} in physical units are connected with their dimensionless counterparts through $\omega = \omega_{ph}/\omega_B$ and $k = k_{ph}c/\omega_B$, Equation (14) is written as

$$\left(-\mathrm{i}\frac{\omega_{ph}}{\omega_B} + \gamma_H\right) \left(-\frac{\omega_{ph}^2}{\omega_B^2} + \frac{k_{ph}^2 c_0^2}{\omega_B^2} - \zeta\frac{k_{ph}^4 c_0^4}{\omega_B^4} - \mathrm{i}\frac{\omega_{ph}}{\omega_B}\gamma_\omega\right) - \mathrm{i}\frac{\omega_{ph}}{\omega_B}m^2 + m^2\gamma_\omega = 0. \tag{15}$$

The real and imaginary parts of the dispersion relation (including losses), Equation (15), are shown in Figure 2 (thin blue solid lines), which are almost the same as the lossless dispersion relation [Equation (15) with $\gamma_\omega \to 0$ and $\gamma_H \to 0$] shown as thick blue solid lines in Figure 2, since we consider a weakly lossy medium.

In addition, in order to verify our theory, we compare this linear dispersion relation with the one obtained by using the Transfer Matrix Method (TMM) [7]. The thin red dashed lines in Figure 2 show the results for the lossy dispersion relation obtained by using the expression given by the TMM method,

$$\cos\left(k_{ph}d\right) = \cos\left(kd\right) + \mathrm{i}\frac{Z_c}{2Z_H}\sin\left(kd\right), \tag{16}$$

where k and Z_c are given by Equations (1) and (2) respectively, and $Z_H = i\omega_{ph}M_H + R_H$ is the input impedance of the side holes. For the lossless case, k, Z_c and Z_H are respectively reduced to $k = \omega/c_0$, $Z_c = \rho_0 c_0/S$ and $Z_H = i\omega_{ph}M_H$, and the corresponding results are shown as thick red dashed lines in Figure 2. The dispersion relation resulting from the continuum approximation (TLM) has a very good agreement with the one obtained by using the TMM, as shown in Figure 2, especially in the low-frequency regime. We note here that while the TLM dispersion relation the losses are approximated by using constant parameters, in the TMM method the loses are frequency dependent. Therefore, the agreement between the two dispersion relations validates our assumption of frequency independent losses.

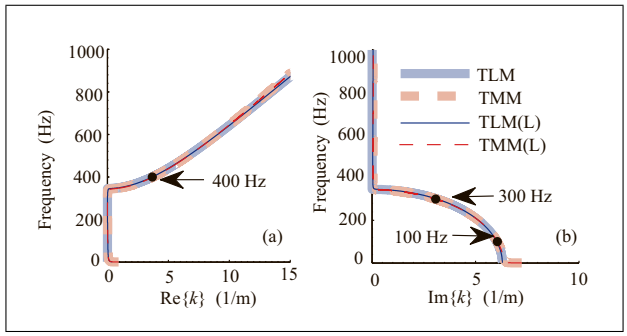

Figure 2. (Colour online) (a) and (b) respectively show the real and imaginary parts of the complex dispersion relation. Blue solid lines (Red dashed lines) show the results obtained by using Transmission line method, Equation (15) (Transfer matrix method, Equation (16)). The thin (thick) solid and dashed lines correspond to the lossy cases (lossless cases). The black points in Figure 2 show the frequencies used in the simulations, 400 Hz, 300 Hz and 100 Hz.

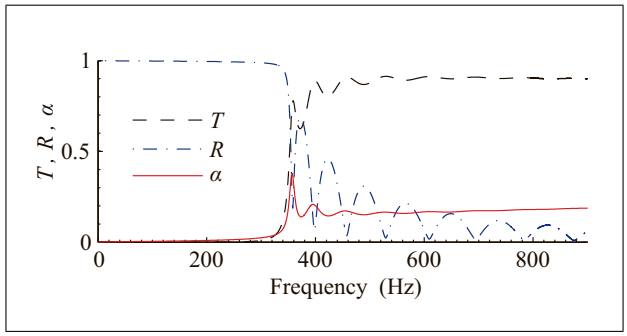

Figure 3. (Colour online) The frequency dependent transmission $|T|$ (black dashed line), reflection $|R|$ (blue dot-dashed line) and absorption $\alpha = 1 - |R|^2 - |T|^2$ (red continuum line) coefficients for a lattice of 1.7 m ($\sim$ 34 cells).

To further validate this assumption, especially for the case of high frequencies (having in mind the generation of the second harmonic), it is relevant to obtain the frequency dependence of the transmission and reflection coefficients, T and R, as well as the absorption coefficient, α, for finite lattice made of 34 cells (1.7 m), as shown in Figure 3, using the TMM method (see details in Appendix A). First, we observe that the transmission and reflection coefficients are in agreement with the dispersion relation shown in Figure 2. Moreover, we find that the absorption coefficient (red continuum line in Figure 3), can be approximated by a constant value in the range of frequencies considered in this work. Therefore, our constant loss assumption –for the frequencies of interest– is well affirmed.

3. Second Harmonic Generation in lossy dispersive acoustic media

In this Section, we study analytically and numerically the second harmonic generation including the effect of the losses.

3.1. Analytical Results

Our analytical methodology relies on a perturbation scheme. First, we express P as an asymptotic series in ϵ, namely

$$P = p_1 + \epsilon p_2 + \epsilon^2 p_3 + \dots . \tag{17}$$

Then, substituting Equation (17) into Equation (12), we obtain a hierarchy of equations at various orders in ϵ. The leading order equation, at $O(\epsilon^0)$,

$$\left(\frac{\partial}{\partial\tau}+\gamma_H\right)\left(\frac{\partial^2 p_1}{\partial\tau^2}-\frac{\partial^2 p_1}{\partial\chi^2}-\zeta\frac{\partial^4 p_1}{\partial\chi^4}+\gamma_\omega\frac{\partial p_1}{\partial\tau}\right) + m^2\frac{\partial p_1}{\partial\tau}+m^2\gamma_\omega p_1 = 0, \tag{18}$$

possesses plane wave solutions of the form,

$$p_1 = A\cos\left(\theta\right), \tag{19}$$

where A is the wave amplitude, $\theta = \omega\tau - k(\omega)\chi$, while parameters k and ω satisfy the dispersion relation $D(\omega, k)$ [cf. Equation (14)]. The equation at the next order, $O(\epsilon^1)$, is

$$\begin{aligned}&\left(\frac{\partial}{\partial\tau}+\gamma_H\right)\left(\frac{\partial^2 p_2}{\partial\tau^2}-\frac{\partial^2 p_2}{\partial\chi^2}-\zeta\frac{\partial^4 p_2}{\partial\chi^4}+\gamma_\omega\frac{\partial p_2}{\partial\tau}\right)\\ &\quad+m^2\frac{\partial p_2}{\partial\tau}+m^2\gamma_\omega p_2 \\ &= -\beta_0\left(-2\mathrm{i}\omega+\gamma_H\right)A^2\left(2\omega^2+\mathrm{i}\gamma_\omega\omega\right)\cos\left(2\omega\tau-2k_1\chi\right).\end{aligned} \tag{20}$$

The solution of Equation (20) is the sum of the particular solution p_2^p of the inhomogeneous equation (forced wave, steady state) and the general solution p_2^g of the homogeneous equation (free wave), namely $p_2 = p_2^p + p_2^g$, with

$$\begin{aligned}p_2^p &= \frac{-\beta_0(-2\mathrm{i}\omega+\gamma_H)A^2(2\omega^2+\mathrm{i}\gamma_\omega\omega)}{D(2\omega,2k)}\\ &\quad\cdot\cos\left(2\omega\tau-2k_1\chi\right), \qquad (21)\\ p_2^g &= p_2^g(\chi=0)\cos\left(2\omega\tau-k_2\chi\right), \qquad (22)\end{aligned}$$

where k_2 is the wavenumber at the second harmonic frequency taken from the dispersion relation. Assuming that the second harmonic vanishes at $x = 0$ and thus $p_2(\tau, \chi = 0) = 0$, we may set

$$p_2^g(\chi=0) = \frac{\beta_0(-2\mathrm{i}\omega+\gamma_H)A^2(2\omega^2+\mathrm{i}\gamma_\omega\omega)}{D(2\omega,2k)}. \tag{23}$$

Thus the full solution for p_2 is written as

$$\begin{aligned}p_2 = p_2^g + p_2^p &= \frac{2\beta_0(-2\mathrm{i}\omega+\gamma_H)A^2(2\omega^2+\mathrm{i}\gamma_\omega\omega)}{D(2\omega,2k)}\\ &\quad\cdot\sin\left(\frac{\Delta k}{2}\chi\right)\sin\left(2\omega\tau-k_{eff}\chi\right),\end{aligned} \tag{24}$$

where Δk is the detuning parameter that describes the asynchronous second harmonic generation, $\Delta k = k(2\omega) - 2k(\omega) = k_2 - 2k_1$, and k_{eff} is the effective wave number, $k_{eff} = (1/2)[k(2\omega) + 2k(\omega)]$.

The presence of β_0 in the amplitude of p_2 shows that, obviously, the second harmonic is generated due to nonlinearity. Since the forced and free waves have different phase velocities, i.e., $2k(\omega) \neq k(2\omega)$, the phase-mismatching introduces a beating in space [26, 27, 43] for the amplitude of the second harmonic –cf. the term $\sin(\Delta k/2\chi)$ in Equation (24). The position of the maximum of the beating $x_c(n)$ can be related to the second harmonic phase-mismatching frequency by $x_c(n) = \pi/\Delta k_n = \pi/|k(n\omega) - nk(\omega)|$, indicating that as Δk_n increases the beating spatial period, and also its maximum amplitude decrease.

3.2. Numerical simulations

We now present results of direct numerical simulations in the framework of the nonlinear discrete model, Equation (9), with and without losses (i.e., $R_H = 0$, $R_\omega = 0$).

The system is excited using a sinusoidal time-depended boundary condition (a driver) at $x = 0$, with an amplitude of 1000 Pa. The length of the lattice is chosen to be long enough in order to avoid reflections from the right end during the evolution.

Using a 4th-order Runge Kutta integrator, we study the propagation for three different driving frequencies. The first case corresponds to a fundamental and a second harmonic, both belonging to the propagating band (Figure 4a and 4b). For the second case, we choose a smaller fundamental frequency lying in the band gap, while the second harmonic lies in the pass band (Figure 4c and 4d). Third, we consider a case where both the fundamental and the second harmonic are in the band gap (Figure 4e and 4f).

We start with the first case where the driver operates at $f = 400$ Hz, and thus both the fundamental component (p_1) and the generated second-harmonic component (p_2) are in the pass band. During the weakly nonlinear wave propagation, in the absence of losses ($R_H = 0, R_\omega = 0, \gamma_H = 0, \gamma_\omega = 0$), the zeroth-order solution p_1 travels with a constant amplitude and a wave vector $k(\omega)$, as shown in Figure 4a (see solid blue line). The second harmonic solution p_2 is composed by a forced wave with $k = 2k(\omega)$ and a free wave propagating with $k(2\omega)$. The phase mismatch, $2k(\omega) \neq k(2\omega)$, introduces beatings in space for the second harmonic, which is shown with the thick blue line in Figure 4b.

We also performed simulations including both the weak viscothermal and radiation losses. The results plotted with the thin (red) lines in Figure 4a and 4b show that the amplitude of both the fundamental and the second harmonics are weakly attenuated. Note that in all cases (with and without losses) our analytical results, shown by the blue stars and red circles, are found to be in a very good agreement with the numerical findings.

When the driving frequency is in the band gap, but close to the cut-off frequency, the generated second harmonic will be located in the pass band. To study such a case, we choose a driver at $f = 300$ Hz. In the lossless case, the fundamental component p_1 decreases exponentially (thick (blue) line in Figure 4c), because the corresponding wavenumber $k(\omega)$ is imaginary (black point in

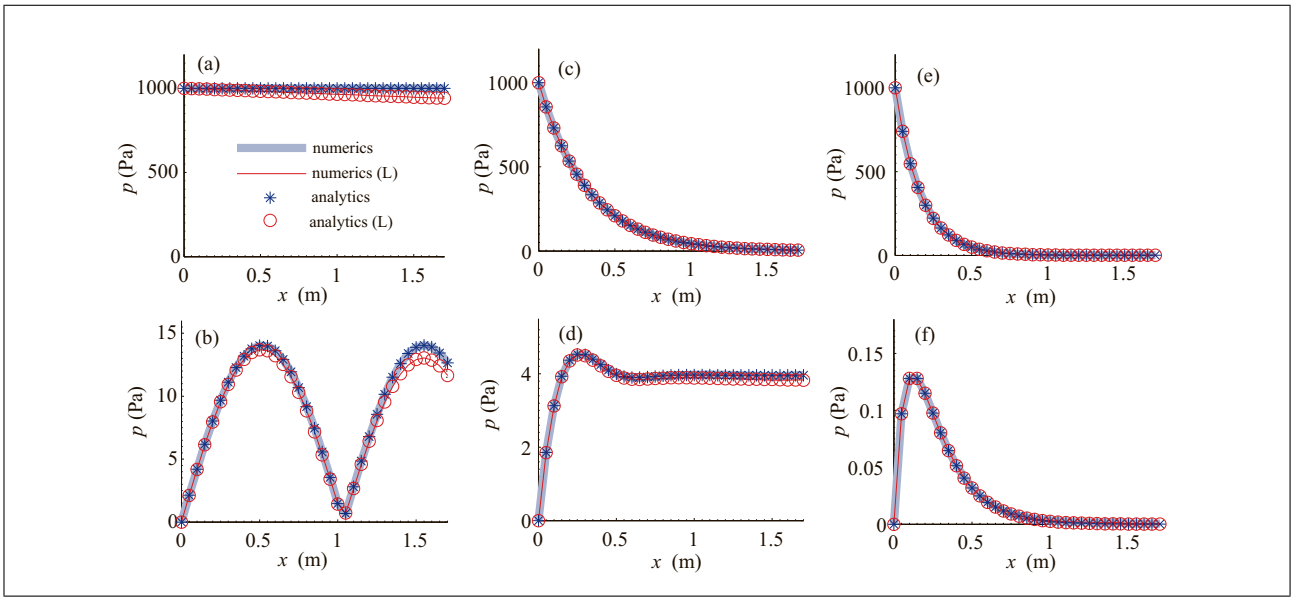

Figure 4. (Colour online) Harmonic generation in the presence of dispersion and (viscothermal and radiation) losses. For the lossy (lossless) case, thin red lines and red circles (thick blue lines and blue stars) stand respectively for the numerical and analytical results. (a) $f = 400$ Hz, p_1 in the pass band; (b) $f = 400$ Hz, p_2 in the pass band; (c) $f = 300$ Hz, p_1 in the band gap; (d) $f = 300$ Hz, p_2 in the pass band; (e) $f = 100$ Hz, p_1 in the band gap; (f) $f = 100$ Hz, p_2 in the band gap. Numerical results are in a good agreement with the analytical ones.

Figure 2b), leading to a strong attenuation of p_1. Since the viscothermal and radiation losses are sufficiently small, we observe almost no difference between the lossless case (thick blue line) and the lossy one (thin red line) in Figure 4c. During propagation, the second harmonic is generated, with a frequency located in the pass band as shown in Figure 4d. Note that the beatings are absent since only the free wave with single wavenumber $k(2\omega)$ is propagating. In this case, we observe a small decrease of the amplitude of p_2 due to the weak viscothermal and radiation losses (thin (red) line in Figure 4d), in comparison to the lossless case (thick (blue) line in Figure 4d).

Finally, in Figure 4e and 4f) we show results corresponding to the third case, i.e., when both the fundamental component p_1 and the second harmonic component p_2 are in the band gap. Here we choose a frequency $f = 100$ Hz for the driver. In this case, the amplitude of p_1 decreases exponentially and faster, as compared to Figure 4c, since the imaginary part of $k(\omega)$ is larger (black point in Figure 2b). The second harmonic is generated at the beginning of the waveguide, but its amplitude eventually decreases to zero, because its frequency is still in the band gap. Since both p_1 and p_2 are in the band gap with relatively large imaginary wavenumbers, the weak viscothermal and radiation losses do not have an important contribution in the evolution, and there is no visible different between the lossless [thick (blue) lines] and lossy [thin (red) lines] propagation, as shown in Figure 4e and 4f).

Note that, in all the cases considered here, numerical results are found to be in a very good agreement with our analytical findings presented in Section 3.1 (blue stars and red circles in Figure 4). At this point, we should mention that during the nonlinear wave propagation, third harmonic is also produced in cascade. However we only consider the second harmonic in this work, because the third harmonic is too small compared to the generated second harmonic. For example, in the lossless case, when our driver is a sinusoidal wave with an amplitude of 1000 Pa and a frequency of 400 Hz, the maximum amplitude of the generated second harmonic is about 14.03 Pa, while the amplitude of the third harmonic is about 0.0307 Pa.

4. Conclusions

In conclusion, we have theoretically and numerically studied second harmonic generation in a 1D weakly lossy nonlinear acoustic metamaterial. The considered structure, composed by an air-filled waveguide loaded with a periodic array of side holes, exhibited viscothermal losses (due to viscous and thermal effects) and radiation losses (due to the side holes). Based on the electro-acoustic analogy, and using the transmission line approach, we derived a nonlinear discrete model describing the propagation of pressure waves. Then, we used a perturbation scheme to analyze the nonlinear dispersive and dissipative wave equation stemming from the long-wavelength limit of the discrete lattice. We have thus derived approximate analytical expressions for the first and second harmonic traveling in the metamaterial. Numerical results were also presented, using a driver, i.e., a sinusodial source, on one end of the waveguide with sufficiently high amplitude.

The numerical results were found to be in a very good agreement with the analytical ones. For the lossless cases, we have shown that during the nonlinear propagation in the metamaterial, the generated higher harmonics could be controlled by tuning the dispersion relation –for instance,

the beatings of second harmonic due to the phase mismatch introduced by the dispersion effect. We also studied the effects of viscothermal and radiation losses on the second harmonic generation in this acoustic metamaterial with negative bulk mudulus. Recently, the second harmonic generation in an one-dimensional, nonlinear acoustic metamaterial with negative mass density, composed of an air-filled waveguide periodically loaded by clamped elastic plates have been analytically and numerically reported [28]. These preliminary results pave the way to study t he nonlinear properties of effective double negative acoustic metamaterials, i.e., an air-filled waveguide periodically loaded with clamped elastic plates and side holes. It would also be interesting to study the nonlinear wave propagation in higher-dimensional acoustic metamaterials.

Acknowledgements

Dimitrios J. Frantzeskakis (D.J.F.) acknowledges warm hospitality at Laboratoire d'Acoustique de l'Université du Maine (LAUM), Le Mans, where most of his work was carried out.

Appendix

A1. Transfer Matrix Method

For a finite lattice of N cells (here, $N = 34$), the total transmission matrix can be expressed as

$$\begin{pmatrix} p_1 \\ u_1 \end{pmatrix} = \left(m_\omega m_H m_\omega\right)^N \begin{pmatrix} p_2 \\ u_2 \end{pmatrix} = \begin{pmatrix} T_{11} & T_{12} \\ T_{21} & T_{22} \end{pmatrix} \begin{pmatrix} p_2 \\ u_2 \end{pmatrix}, \tag{A1}$$

with

$$m_\omega = \begin{pmatrix} \cos(kd/2) & \mathrm{j}Z_c \sin(kd/2) \\ \frac{\mathrm{j}}{Z_c}\sin(kd/2) & cos(kd/2) \end{pmatrix}, \tag{A2}$$

$$m_H = \begin{pmatrix} 1 & 0 \\ (\mathrm{i}\omega M_H + R_H)^{-1} & 1 \end{pmatrix}, \tag{A3}$$

where $p_1(u_1)$ and $p_2(u_2)$ are the pressure (volume velocity) at the input and output of the settings. Then the transmission coefficient (T) and reflection one (R) can be calculated respectively as

$$T = \frac{2}{T_{11} + T_{12}/Z_c + T_{21}Z_c + T_{22}}, \tag{A4}$$

$$R = \frac{T_{11} + T_{12}/Z_c - T_{21}Z_c - T_{22}}{T_{11} + T_{12}/Z_c + T_{21}Z_c + T_{22}}. \tag{A5}$$

The absorption coefficient α is $\alpha = 1 - |T|^2 - |R|^2$.

References

[1] V. G. Veselago: The electrodynamics of substances with simultaneously negative values of ϵ and μ. Soviet physics uspekhi **10(4)** (1968) 509.

[2] R. A. Shelby, D. R. Smith, S. Schultz: Experimental verification of a negative index of refraction. Science **292** (2001) 5514.

[3] A. A. Houck, J. B. Brock, I. L. Chuang: Experimental observations of a left-handed material that obeys Snell's Law. Phys. Rev. Lett. **90** (2003) 137–401.

[4] Z. Liu, X. Zhang, Y. Mao, Y. Y. Zhu, Z. Yang, C. T. Chan, P. Sheng: Locally resonant sonic materials. Science **289** (2000) 1734.

[5] N. Fang, D. Xi, J. Xu, M. Ambati, W. Srituravanich, C. Sun, X. Zhang: Ultrasonic metamaterials with negative modulus. Nat. Mater. **5** (2006) 452.

[6] N. Sugimoto, T. Horioka: Dispersion characteristics of sound waves in a tunnel with an array of Helmholtz resonators. J. Acoust. Soc. Am. **97** (1995) 1446.

[7] C. E. Bradly: Time harmonic acoustic Bloch wave propagation in periodic waveguides. Part I. Theory. J. Acoust. Soc. Am. **96** (1994) 1844.

[8] C. Zwikker, C.W.Kosten: Sound absorbing materials. Elsevier, New York, 1949.

[9] C. E. Bradly: Time harmonic acoustic Bloch wave propagation in periodic waveguides. Part II. Experiment. J. Acoust. Soc. Am. **96(3)** (1994) 1854–1862.

[10] L. Solymar, E. Shamonina: Waves in Metamaterials. Oxford University Press, New York, 2009.

[11] G. Theocharis, O. Richoux, V. R. GarcÃŋa, A. Merkel, V. Tournat: Limits of slow sound propagation and transparency in lossy, locally resonant periodic structures. New J. of Phys **16(9)** (2014) 093017.

[12] G. Ma, M. Yang, S. Xiao, Z. Yang, P. Sheng: Acoustic metasurface with hybrid resonances. Nature Mater. **13** (2014) 873–878.

[13] V. Romero-García, G. Theocharis, O. Richoux, A. Merkel, V. Tournat, V. Pagneux: Perfect and broadband acoustic absorption by critically coupled sub-wavelength resonators. Sci. Rep. **6** (2016) 19519.

[14] A. Merkel, G. Theocharis, O. Richoux, V. Romero-García, V. Pagneux: Control of acoustic absorption in one-dimensional scattering by resonant scatterers. Appl. Phys. Lett. **107**, (2015) 244102.

[15] N. Jiménez, W. Huang, V. Romero-García, V. Pagneux, J.-P. Groby: Ultra-thin metamaterial for perfect and quasi-omnidirectional sound absorption Appl. Phys. Lett. **109**, (2016) 121902.

[16] Noé Jiménez, Vicent Romero-García, Vincent Pagneux, Jean-Philippe Groby: Quasiperfect absorption by subwavelength acoustic panels in transmission using accumulation of resonances due to slow sound. Phys. Rev. B **95**, (2017) 014205.

[17] Mikhail Lapine, Ilya V. Shadrivov, Yuri S. Kivshar: Colloquium: Nonlinear metamaterials, Rev. Mod. Phys. **86**, (2014) 1093.

[18] M. I. Shalaev, S. A. Myslivets, V. V. Slabko, A. K. Popov: Negative group velocity and three-wave mixing in dielectric crystals. Optics letters **36(19)** (2011) 3861–3863.

[19] Jacob B. Khurgin: Optical parametric oscillator: Mirrorless magic. Nat Photon. **1** (2007) 446–447.

[20] A. K. Popov, V. V. Slabko, V. M. Shalaev: Second harmonic generation in left-handed metamaterials. Laser Physics Letters. **3**(6) (2006) 293.

[21] N. Sugimoto, M. Masuda, J. Ohno, D. Motoi: Experimental demonstration of generation and propagation of acous-

tic solitary waves in an air-filled tube. Phys. Rev. Lett. **83** (1999) 4053.

[22] O. Richoux, B. Lombard, J. F. Mercier: Generation of acoustic solitary waves in a lattice of Helmholtz resonators. Wave Motion **56** (2015) 85–99.

[23] V. Achilleos, O. Richoux, G. Theocharis, D. J. Frantzeskakis: Acoustic solitons in waveguides with Helmholtz resonators: Transmission line approach. Phys. Rev. E **91** (2015) 023204.

[24] M. A. Averkiou, Y. S. Lee, M. F. Hamilton: Self-demodulation of amplitude and frequency modulated pulses in a thermoviscous fluid. J. Acoust. Soc. Am. **94**(5) (1993) 2876–2883.

[25] H. J. Vos, D. E. Goertz, N. de Jong: Self-demodulation of high-frequency ultrasound. J. Acoust. Soc. Am. **127**(3) (2010) 1208–1217.

[26] V. J. Sánchez-Morcillo, I. Pérez-Arjona, V. Romero-García, V. Tournat, V. E. Gusev: Second-harmonic generation for dispersive elastic waves in a discrete granular chain. Phys. Rev. E **88** (2013) 043203.

[27] N. Jiménez, A. Mehrem, R. Picó, L. M. García-Raffi, V. J. Sánchez-Morcillo: Nonlinear propagation and control of acoustic waves in phononic superlattices. C. R. Phys. **17** (2016) 543–554.

[28] J. Zhang, V. Romero-García, G. Theocharis, O. Richoux, V. Achilleos, D. J. Frantzeskakis: Second-Harmonic Generation in Membrane-Type Nonlinear Acoustic Metamaterials. Crystals **6**(8) (2016) 86.

[29] J. Zhang, V. Romero-García, G. Theocharis, O. Richoux, V. Achilleos, D. J. Frantzeskakis: Bright and Gap Solitons in Membrane-Type Acoustic Metamaterials. Phys. Rev. E **96** (2017) 022214.

[30] F. Bongard, H. Lissek, J. R. Mosig: Acoustic transmission line metamaterial with negative/zero/positive refractive index. Phys. Rev. B **82** (2010) 094306.

[31] C. M. Park, J. J. Park, S. H. Lee, Y. M. Seo, C. K. Kim, S. H. Lee: Amplification of acoustic evanescent waves using metamaterial slabs. Phys. Rev. Lett. **107** (2011) 194301.

[32] K. J. B. Lee, M. K. Jung, S. H. Lee: Highly tunable acoustic metamaterials based on a resonant tubular array. Phys. Rev. B **86** (2012) 184302.

[33] R. Fleury, A. Alú: Extraordinary sound transmission through density-near-zero ultranarrow channels. Phys. Rev. Lett. **111** (2013) 055501.

[34] T. D. Rossing, N. H. Fletcher: Principles of Vibration and Sound. Springer-Verlag, New York, United States of America, 1995.

[35] L. E. Kinsler, A. U. Frey, A. B. Coppens, J. V. Sanders: Fundamentals of Acoustics. Whiley, New York, 1982.

[36] M. Rossi: Acoustics and Electroacoustics. Artech House, Norwood, MA, 1988.

[37] P. A. Kalozoumis, O. Richoux, F. K. Diakonos, G. Theocharis, P. Schmelcher: Invariant currents in lossy acoustic waveguides with complete local symmetry. Phys. Rev. B **92** (2015) 014303.

[38] M. Atig, J. P. Dalmont, J. Gilbert: Termination impedance of open-ended cylindrical tubes at high sound pressure level. Comptes Rendus Mécanique **332**(4) (2004) 299–304.

[39] J. M. Buick, M. Atig, D. J. Skulina, D. M. Campbell, J. P.Dalmont, J. Gilbert: Investigation of non-linear acoustic losses at the open end of a tube. J. Acoust. Soc. Am. **129(3)** (2011) 1261–72.

[40] M. Remoissenet: Waves called solitons. Springer, Berlin, Germany, 1999.

[41] M. J. Ablowitz: Nonlinear Dispersive waves, asymptotic analysis and solitons. Cambridge texts in applied mathematics, Cambridge University Press, New York, 2011.

[42] M. F. Hamilton, D. T. Blackstock: Nonlinear Acoustics. Academic Press, AIP, San Diego, California, United States of America, 1998.

[43] A. Mehrem, N. Jiménez, L. J. Salmerón-Contreras, X. García-Andrés, L. M. García-Raffi, R. PicÃş, V. J. Sánchez-Morcillo: Nonlinear dispersive waves in repulsive lattices. Phys. Rev. E **96** (2017) 012208.